Near- and far-field boundary conditions for a finite element method for the Helmholtz equation in axisymmetric problems of underwater acoustics

Dimitrios A. Mitsoudis
Department of Applied Mathematics, University of Crete,
71409 Heraklion, Greece
e-mail: dmits@tem.uoc.gr
and
Institute of Applied and Computational Mathematics,
FO.R.T.H., P.O. Box 1527, 71110 Heraklion, Greece

Abstract

We consider the Helmholtz equation in a stratified cylindrically symmetric waveguide overlying a rigid bottom. Nonlocal boundary conditions are posed at a near- and a far-field artificial boundary. At the near-field boundary a nonhomogeneous DtN-type condition that takes into account the effects of the source and of the backscattering from the rest of the waveguide is posed. At the far-field boundary is used a condition associated with the DtN map of the exterior problem. The problem is discretized by a standard Galerkin/finite element method and is implemented in a Fortran code called FENL^2. The code is tested on some small scale problems and its results are compared with those of COUPLE and are found to be in excellent agreement.

PACS no. 43.20.Bi, 43.20.Fn, 43.30.Gv

Short title: Near- and far-field nonlocal boundary conditions.

1 Introduction

The numerical solution of problems governed by the Helmholtz equation is still recognized as an interesting and challenging task. In this paper we shall deal with applications in underwater

acoustics, where the Helmholtz equation models the propagation of the sound field due to a source that generates a continuous, time-harmonic signal. Specifically, we consider a cylindrically symmetric waveguide consisting, for simplicity, of two fluid layers of different acoustic parameters overlying a rigid bottom. Due to the axial symmetry it is convenient to introduce a cylindrical coordinate system with its vertical axis passing through the source. The precise boundary-value problem that we consider will be stated in the next section.

We shall use a finite element method to solve the problem, since this class of direct numerical methods has been proved efficient in solving problems characterized by features such as medium inhomogeneities, discontinuous coefficients, large discrepancies in the acoustic parameters of the different layers and/or complex interface and bottom topographies. Of course, our domain is unbounded so in order to discretize it we have to truncate it and formulate an equivalent problem posed in the bounded part of the waveguide. This may be succeeded by introducing two artificial boundaries at suitable values of range, near and far from the source, assuming that all the range dependent features of the problem are localized in the bounded part of the waveguide confined by these two boundaries, while near the source and in the exterior far-field region the problem is range-independent enabling us to obtain analytic representations of the sound field, which in turn are used to derive appropriate boundary conditions at the artificial boundaries. At the far-field boundary the *Dirichlet-to-Neumann* (DtN) condition may be posed, while at the near-field boundary another nonhomogeneous DtN-type condition may be derived, relating the source field to the field in the rest of the waveguide.

For the far-field boundary this approach was first adopted for problems in underwater acoustics by Fix and Marin in [1], where they studied the case of a single layer axially symmetric waveguide. Goldstein in [2] gave a convergence proof for a finite element method coupled with an exact nonlocal boundary condition posed on an artificial boundary in a single layer waveguide in Cartesian coordinates. The term DtN for this kind of exact non reflecting boundary conditions has been established by Keller and Givoli in [3], where they constructed DtN conditions for exterior problems in two and three dimensions. We refer to the book of Givoli, [4], for further information on related work. We also refer to the paper by Thompson, [5], for a recent review of finite element methods for problems governed by the Helmholtz equation, and to the paper by Buckingham, [6], where a thorough report of various ocean-acoustic propagation models and their special features may be found.

Another class of methods that have been used extensively in underwater acoustics is coupled

mode methods, which extend the classical normal mode expansion of the acoustic field in a horizontally stratified medium, see e.g. [7], or [8], in order to approximate the solution of problems in range-dependent waveguides. Evans, in [9], constructed a coupled-mode model and an associated code called COUPLE, see [10], which subdivides the waveguide into a sequence of range-independent regions (using the staircase approximation to discretize variable interfaces and bottom) and represents the acoustic field as a normal-mode series in each column. Then, continuity of pressure and horizontal particle velocity is used across the inter-element vertical interfaces resulting to a full two-way solution in terms of coupled modes. However, in case of highly irregular interface or bottom topographies a large number of horizontal staircase steps should be accounted for accuracy purposes leading to slow-rate of convergence. Over the last two decades or so, some other coupled-mode approaches have been proposed trying to improve the treatment of irregular bottom or interface topographies. Indicatively we refer to Rutherford and Hawker, [11], Taroudakis et al., [12], Fawcett, [13], and Athanassoulis and Belibassakis, [14].

In the present paper we use a standard Galerkin discretization of the Helmholtz equation coupled to nonlocal nonreflecting boundary conditions posed on two artificial boundaries near the source and far from the source. This method is implemented in a code called FENL^2, which is a modified version of a code called FENL, originally written by Kampanis and Dougalis, see [15]. In the prototype code FENL a Galerkin finite element discretization of the Helmholtz equation in an axially symmetric two layer waveguide coupled with a DtN boundary condition posed on a far-field boundary was implemented. At the near-field boundary a nonhomogeneous Dirichlet boundary condition (of the form $u = g$) was used to approximate the acoustic field u generated by the time-harmonic point source, where g was a given (complex) function of depth. In practice the computed field by a coupled mode method was used as a boundary condition on the inner artificial boundary. Thus, the FENL code was not self-contained and of course depended on the modal data given on the near-field artificial boundary. FENL has been tested and compared to other codes quite extensively. In [15] the code was tested on several small scale examples and its results were compared with those of COUPLE. In [16], an earlier version of FENL was compared to a coupled mode code, called MODE4, developed by Taroudakis. In [17] there has been performed a detailed comparison between the results of FENL with those of a coupled mode method (CCMM) by Athanassoulis and Belibassakis, [14], and also of COUPLE. It was found out that, in general, the results of the three codes compared very well, but at some frequencies increased discrepancies between FENL and the normal mode

codes were observed. To be more specific, we have found that for some source frequencies for which some eigenvalue of the local, vertical eigenvalue problem changed sign several times in the neighbourhood of the inhomogeneity in the interface topography, the accuracy of the FENL computations was depending on the position where the near-field (inflow) boundary was posed. In FENL^2, in order to avoid resonances due to the use of a modal starter, we have replaced the nonhomogeneous Dirichlet boundary condition on the near-field boundary by an appropriate nonhomogeneous DtN-type condition. This renders FENL^2 a self-contained finite element code.

This paper is organized as follows: In Section 2 the geometry of the waveguide is specified and we formulate the original problem in the semi-infinite waveguide. Next, we introduce two artificial boundaries near the source and far from the source, that allow us to define a boundary-value problem in a bounded domain which is equivalent to the original one, and we describe the derivation of the DtN boundary conditions that we pose on them. In Section 3 we introduce the suitable function space setting and describe the finite element method that is used to discretize the boundary-value problem. Then, we briefly outline the code FENL^2, which implements the finite element discretization, and the various software packages to which it is coupled. In Section 4 we present results of three numerical experiments that we performed with the code in underwater waveguides consisting of two fluid layers, where the interface simulates an upslope, a downslope and an underwater hill environment. In order to validate the code we have compared our results with those of COUPLE, which is considered as the established benchmark code for range-dependent problems. In all cases the results of the two codes were found to be in excellent agreement.

2 Formulation of the problem

In this section we briefly present the formulation of the boundary-value problem that we are going to study in the sequel. We consider a cylindrically symmetric waveguide consisting, for simplicity, of two fluid layers overlying a rigid bottom, see Figure 1. A cylindrical coordinate system is introduced with its origin placed at the free-surface and the vertical z–axis being positive downwards. The surface ($z = 0$) is assumed to be horizontal, while the interface and the bottom, denoted by $\Gamma_{\rm int}$ and $\Gamma_{\rm bot}$, respectively, may vary with range.

Figure 1 is here.

The upper layer $\Omega_1 := \Omega_{\rm N}^{\rm w} \cup \Omega^{\rm w} \cup \Omega_{\rm F}^{\rm w}$ represents the water column of constant density equal to $\rho_{\rm w}$, while the lower one $\Omega_2 := \Omega_{\rm N}^{\rm s} \cup \Omega^{\rm s} \cup \Omega_{\rm F}^{\rm s}$ represents the sediment layer which is also of constant density equal to $\rho_{\rm s}$ ($\rho_{\rm s} > \rho_{\rm w}$). We point out that there is no attenuation neither in the water column nor in the sediment layer. We also assume that the domain of the problem consists of three parts: (a) The near-field bounded subdomain $\Omega_{\rm N} := \Omega_{\rm N}^{\rm w} \cup \Omega_{\rm N}^{\rm s}$ (for $0 \le r \le r_{\rm N}$), where the interface and the bottom are assumed to be horizontal at constant depths $z = h_{\rm N}$ and $z = H_{\rm N}$, respectively, (b) the intermediate bounded subdomain Ω (for $r_{\rm N} < r < r_{\rm F}$), and (c) the far-field, unbounded subdomain $\Omega_{\rm F} := \Omega_{\rm F}^{\rm w} \cup \Omega_{\rm F}^{\rm s}$ (for $r \ge r_{\rm F}$), where the interface and the bottom are also assumed to be horizontal at constant depths $z = h_{\rm F}$ and $z = H_{\rm F}$, respectively.

The sound speed is taken to be independent of r in $\Omega_{\rm N}$ and $\Omega_{\rm F}$ (i.e. $c = c_{\rm N}(z)$ in $\Omega_{\rm N}$ and $c = c_{\rm F}(z)$ in $\Omega_{\rm F}$), and varies smoothly from its near-field to its far-field value within each layer in the intermediate subdomain Ω. The sound field is generated by a time-harmonic point source of frequency f placed at $r = 0$ at a depth equal to $z_{\rm s}$, where $0 < z_{\rm s} < h_{\rm N}$ (i.e. it is assumed that the source is located in the water column).

The formulation of the acoustic propagation problem in such an environment is well-known, we refer e.g. to [8], [7]. The acoustic field (acoustic pressure) satisfies in each layer the Helmholtz equation

$$\Delta u(r,z) + k^2(r,z)\, u(r,z) = -\frac{1}{2\pi r}\, \delta(r)\, \delta(z - z_{\rm s}), \tag{1}$$

where $\Delta u = u_{rr} + \frac{1}{r}\, u_r + u_{zz}$ (there is no dependence on the azimuth θ due to the axial symmetry) and $k\,(r,z) = \omega / c\,(r,z)$ is the (real) wavenumber. Equation (1) is supplemented by boundary and interface conditions. On the surface a homogeneous Dirichlet boundary condition (pressure release) $u = 0$ is posed. The bottom is assumed to be acoustically hard, i.e. a Neumann condition $\frac{\partial u}{\partial n} = 0$ holds. Across the interface the usual conditions hold, i.e. u is continuous across $\Gamma_{\rm int}$, and $\frac{1}{\rho_{\rm w}} \frac{\partial u}{\partial n}\Big|_{\Gamma_{\rm int}-} = \frac{1}{\rho_{\rm s}} \frac{\partial u}{\partial n}\Big|_{\Gamma_{\rm int}+}$, where n is the outward normal of the water layer to the variable interface, and the $\mp$ symbols denote that the functions are evaluated at $\Gamma_{\rm int}$ by their limits from $\Omega^{\rm w}$ and $\Omega^{\rm s}$, respectively. Finally, a radiation condition is posed yielding that $u(r,z)$ behaves like an outgoing cylindrical wave as $r \to \infty$.

2.1 Reformulation of the problem in a bounded domain

Since we are interested in solving the previously described problem with a direct numerical method we have to truncate the semi-infinite domain and reformulate the original problem to an equivalent in a bounded domain. One way to do this is to introduce two artificial boundaries.

The first, denoted by Γ_4, is placed at a distance $r = R_1$, where $0 < R_1 < r_{\rm N}$, and will be referred as the near-field boundary, and the second denoted by Γ_2, is placed at a distance $r = R_2$, where $R_2 > r_{\rm F}$, and will be referred as the far-field boundary. We shall also denote by Γ_1, Γ_3, and $\Gamma_{\rm i}$ the parts of the bottom, the surface and the interface, respectively, lying between the cylinders $r = R_1$ and $r = R_2$. Therefore, the boundary of the computational domain $\Omega := \Omega^{\rm w} \cup \Omega^{\rm s}$ is defined as $\partial\Omega := \Gamma_1 \cup \Gamma_2 \cup \Gamma_3 \cup \Gamma_4$. Now, suitable boundary conditions have to be posed on the artificial boundaries. At the near-field boundary Γ_4 a condition relating at $r = R_1$ the acoustic field generated by the time-harmonic point source to the backscattered field from the rest of the waveguide may be posed. At the far-field boundary Γ_2 a 'transparent' condition should be posed, i.e. a condition which allows outgoing waves to pass through the artificial boundary Γ_2 without producing any spurious reflections.

Then the original problem may be written as follows: We seek a complex-valued function $u(r, z)$, $(r, z) \in \overline{\Omega}$, such that

$$\Delta u + k^2(r, z)u = 0 \ \text{ in } \Omega^{\rm w} \cup \Omega^{\rm s}, \tag{2}$$

$$u\,|_{\Gamma_{\rm i}-} = u\,|_{\Gamma_{\rm i}+}, \tag{3}$$

$$\frac{1}{\rho_{\rm w}} \frac{\partial u}{\partial n}\bigg|_{\Gamma_{\rm i}-} = \frac{1}{\rho_{\rm s}} \frac{\partial u}{\partial n}\bigg|_{\Gamma_{\rm i}+}, \tag{4}$$

$$\frac{\partial u}{\partial n} = 0 \text{ on } \Gamma_1, \tag{5}$$

$$\frac{\partial u}{\partial r} = T(u) \text{ on } \Gamma_2, \tag{6}$$

$$u = 0 \text{ on } \Gamma_3, \tag{7}$$

$$\frac{\partial u}{\partial r} = R(u) + S \text{ on } \Gamma_4. \tag{8}$$

The operator T appearing in (6) is the DtN integral operator associated with the exterior acoustic field, the operator R in (8) is another integral operator relating the fields in Ω and in the near-field region $\Omega_{\rm N}$, and S is a function of z. In the sequel we shall present the derivation of these conditions.

2.2 Inflow and outflow boundary conditions

In order to construct the inflow and outflow boundary conditions we follow the approach of Evans, [9], to obtain analytic representations of the acoustic field in the near- and the far-field domains $\Omega_{\rm N}$ and $\Omega_{\rm F}$, respectively (see also Jensen et al., [8]):

In the *near-field* region, i.e. for $(r,z) \in \Omega_{\rm N}$, we get that

$$u(r,z) = \sum_{n=1}^{\infty} \alpha_n \, J_0(\sqrt{\lambda_n^{\rm N}} r) \, Z_n^{\rm N}(z) + \frac{\mathrm{i}}{4\rho_{\rm w}} \sum_{n=1}^{\infty} H_0^{(1)}(\sqrt{\lambda_n^{\rm N}} r) \, Z_n^{\rm N}(z_{\rm s}) \, Z_n^{\rm N}(z). \tag{9}$$

In the *far-field* region, i.e. for $(r,z) \in \Omega_{\rm F}$, it holds that

$$u(r,z) = \sum_{n=1}^{\infty} \beta_n \, H_0^{(1)}(\sqrt{\lambda_n^{\rm F}} r) \, Z_n^{\rm F}(z). \tag{10}$$

In (9) J_0 is the Bessel function of zero order, $H_0^{(1)}$ is the Hankel function of the first kind and zero order, and the first series is a solution of the homogeneous counterpart of Equation (1), while the second series may be viewed as the source term. In (10) only Hankel functions of the first kind are present due to the radiation condition. Furthermore, $\{\lambda_n^*, Z_n^*(z)\}$, $n = 1, 2, \ldots$, are the eigenvalues and the corresponding eigenfunctions of the two-point vertical eigenvalue problem

$$\frac{d^2 Z_n^*}{dz^2} + \left(k_*^2(z) - \lambda_n^*\right) \, Z_n^* = 0 \quad \text{ in } [0, h_*) \cup (h_*, H_*], \tag{11}$$

$$Z_n^*(0) = 0, \tag{12}$$

$$Z_n^*(h_*-) = Z_n^*(h_*+), \tag{13}$$

$$\frac{1}{\rho_{\rm w}} \frac{dZ_n^*}{dz}(h_*-) = \frac{1}{\rho_{\rm s}} \frac{dZ_n^*}{dz}(h_*+), \tag{14}$$

$$\frac{dZ_n^*}{dz}(H_*) = 0, \tag{15}$$

where, here and in the sequel, in place of the asterisk $*$, we read N in the near-field region $\Omega_{\rm N}$, and F in the far-field region $\Omega_{\rm F}$.

We assume that the problem (11)–(15) is such that $\lambda_n^* \neq 0$, for all n. It is well-known that the eigenvalues of this problem are real and form a decreasing sequence such that

$$\max_{z \in [0, H_*]} k_*^2(z) \geq \lambda_1^* \geq \lambda_2^* \geq \ldots \geq \lambda_n^* \to -\infty.$$

Let us assume that N_* is a positive integer such that $\lambda_n^* > 0$, for $n = 1, \ldots, N_*$ (i.e. correspond to the *propagating* modes), and $\lambda_n^* < 0$, for $n = N_* + 1, N_* + 2, \ldots$ (i.e. correspond to the *evanescent* modes). We should like to note that we follow the convention that the square root $\sqrt{\mu}$, for μ real, is taken to be equal to $\sqrt{\mu}$, if $\mu \geq 0$, and to $i\sqrt{-\mu}$, if $\mu < 0$.

We also assume that the eigenfunctions Z_n^* are orthonormal with respect to the weighted L^2-inner product

$$(w, u)_{L^2_\rho(0,H_*)} := \int_0^{h_*} w \, \overline{u} \, dz + \rho \int_{h_*}^{H_*} w \, \overline{u} \, dz,$$

where $\rho := \frac{\rho_{\rm w}}{\rho_{\rm s}}$.

Now, we consider a fixed $r' \in (0, r_{\rm N})$, we take the inner product of u and $Z_m^{\rm N}$ with respect to $(\cdot,\cdot)_{L^2_\rho(0,H_{\rm N})}$, and we use Equation (9) and the orthonormality of $Z_n^{\rm N}$, $n = 1, 2, \ldots$, to obtain immediately that the coefficients α_n satisfy the following relation

$$\alpha_n = \frac{1}{J_0(\sqrt{\lambda_n^{\rm N}} r')} \left[\Big(u(r', \cdot), Z_n^{\rm N} \Big)_{L^2_\rho(0,H_{\rm N})} - \frac{\rm i}{4\rho_{\rm w}} H_0^{(1)}(\sqrt{\lambda_n^{\rm N}} r')\, Z_n^{\rm N}(z_s) \right], \text{ for } 0 < r' < r_{\rm N}. \quad (16)$$

Similarly, for $r' > r_{\rm F}$, Equation (10) and the orthonormality of $Z_n^{\rm F}$, $n = 1, 2, \ldots$, with respect to $(\cdot,\cdot)_{L^2_\rho(0,H_{\rm F})}$, implies that the coefficients β_n in (10) are given by

$$\beta_n = \frac{1}{H_0^{(1)}(\sqrt{\lambda_n^{\rm F}} r')} \Big(u(r', \cdot), Z_n^{\rm F} \Big)_{L^2_\rho(0,H_{\rm F})}, \text{ for } r' > r_{\rm F}. \quad (17)$$

Next, we differentiate (9) with respect to r, and we evaluate the resulting expression at $r = R_1$. Using (16) and some properties of the special functions that are involved, we deduce that the nonlocal inflow condition on Γ_4 may be written in the form

$$\frac{\partial u}{\partial r}(R_1, z) = R(u)(z) + S(z), \quad (18)$$

where

$$R(u)(z) := \sum_{n=1}^{\infty} a_n(u)\, Z_n^{\rm N}(z), \quad (19)$$

$$S(z) := -\frac{1}{2\pi\rho_{\rm w} R_1} \sum_{n=1}^{\infty} \frac{1}{J_0(\sqrt{\lambda_n^{\rm N}} R_1)}\, Z_n^{\rm N}(z_{\rm s})\, Z_n^{\rm N}(z), \quad (20)$$

and

$$a_n(u) = \sqrt{\lambda_n^{\rm N}} \frac{J_0'(\sqrt{\lambda_n^{\rm N}} R_1)}{J_0(\sqrt{\lambda_n^{\rm N}} R_1)} \Big(u(R_1, \cdot), Z_n^{\rm N} \Big)_{L^2_\rho(0,H_{\rm N})}.$$

Analogously, the DtN map of the acoustic field in the exterior region $\Omega_{\rm F}$, evaluated on Γ_2, is

$$\frac{\partial u}{\partial r}(R_2, z) = T(u)(z) := \sum_{n=1}^{\infty} b_n(u)\, Z_n^{\rm F}(z), \quad (21)$$

where

$$b_n(u) = \sqrt{\lambda_n^{\rm F}} \frac{H_0^{(1)'}(\sqrt{\lambda_n^{\rm F}} R_2)}{H_0^{(1)}(\sqrt{\lambda_n^{\rm F}} R_2)} \Big(u(R_2, \cdot), Z_n^{\rm F} \Big)_{L^2_\rho(0,H_{\rm F})}.$$

In the sequel, we shall assume that the boundary-value problem (2)–(8) has a unique solution and we refer to [2], and the references therein, for well-posedness results in the case of a perturbed single-layer semi-infinite cylindrical waveguide.

3 The finite element method

In the present section we shall show how to approximate the solution of the problem (2)–(8) with the standard Galerkin/finite element method. In order to do so, we have to obtain a weak formulation. First, we introduce some notation. Let $\overset{0}{\mathcal{H}}(\Omega, \Gamma_3)$ be the space of complex-valued functions u of r and z, defined on $\overline{\Omega}$, such that

$$\int_{\Omega^{\rm w}} |u|^2 \, r \, dr dz + \rho \int_{\Omega^{\rm s}} |u|^2 \, r \, dr dz < \infty$$

and

$$\int_{\Omega^{\rm w}} (|u_r|^2 + |u_z|^2) \, r \, dr dz + \rho \int_{\Omega^{\rm s}} (|u_r|^2 + |u_z|^2) \, r \, dr dz < \infty,$$

and vanishing on Γ_3.

Then, the weak form of the boundary-value problem (2)–(8) is the following:
Seek $u \in \overset{0}{\mathcal{H}}(\Omega, \Gamma_3)$ such that

$$\begin{aligned} &-(\nabla u, \nabla v)_{L^2_\rho(\Omega)} + (k^2 u, v)_{L^2_\rho(\Omega)} \\ &+(T(u), v)_{L^2_\rho(\Gamma_2)} - (R(u), v)_{L^2_\rho(\Gamma_4)} = (S, v)_{L^2_\rho(\Gamma_4)}, \end{aligned} \tag{22}$$

for all $v \in \overset{0}{\mathcal{H}}(\Omega, \Gamma_3)$. The operators R and T are defined by (19) and (21), respectively, the function S by (20), $(\nabla u, \nabla v)_{L^2_\rho(\Omega)} := (u_r, v_r)_{L^2_\rho(\Omega)} + (u_z, v_z)_{L^2_\rho(\Omega)}$, and

$$\begin{aligned} (u, v)_{L^2_\rho(\Omega)} &:= \int_{\Omega^{\rm w}} u \, \overline{v} \, r \, dr dz + \rho \int_{\Omega^{\rm s}} u \, \overline{v} \, r \, dr dz, \\ (u, v)_{L^2_\rho(\Gamma_4)} &:= \int_0^{h_{\rm N}} u \, \overline{v} \, R_1 \, dz + \rho \int_{h_{\rm N}}^{H_{\rm N}} u \, \overline{v} \, R_1 \, dz, \\ (u, v)_{L^2_\rho(\Gamma_2)} &:= \int_0^{h_{\rm F}} u \, \overline{v} \, R_2 \, dz + \rho \int_{h_{\rm F}}^{H_{\rm F}} u \, \overline{v} \, R_2 \, dz, \end{aligned}$$

where $\rho = \rho_{\rm w}/\rho_{\rm s}$. We shall assume that (22) has a unique solution.

Let $\mathcal{T}_h$ denote a triangulation of Ω with triangles of maximum sidelength h. We discretize (22) by the finite element method with continuous in Ω piecewise linear functions defined on $\mathcal{T}_h$. For simplicity, we assume that the interface and the bottom consist of straight line segments; thus $\Omega^{\rm w}$ and $\Omega^{\rm s}$ are polygonal domains. We introduce the finite element space

$$\overset{0}{V}_h := \{\phi : \ \phi \in C(\overline{\Omega}), \ \phi = 0 \text{ on } \Gamma_3, \ \phi \,|_\tau \in \mathbb{P}_1 \ \ \forall \, \tau \in \mathcal{T}_h\}.$$

The space $\overset{0}{V}_h$ is a finite dimensional subspace of $\overset{0}{\mathcal{H}}(\Omega, \Gamma_3)$. Then the discrete analog of (22) is the following: Seek $u_h \in \overset{0}{V}_h$, such that

$$\begin{aligned} &-(\nabla u_h, \nabla \phi)_{L^2_\rho(\Omega)} + (k^2 u_h, \phi)_{L^2_\rho(\Omega)} \\ &+(\widetilde{T} u_h, \phi)_{L^2_\rho(\Gamma_2)} - (\widetilde{R} u_h, \phi)_{L^2_\rho(\Gamma_4)} = (\widetilde{S}, \phi)_{L^2_\rho(\Gamma_4)}, \end{aligned} \tag{23}$$

for all $\phi \in \overset{0}{V}_h$. Here $\widetilde{R}$, $\widetilde{S}$ and $\widetilde{T}$ are discrete approximations of R, S and T obtained by truncating the series in (19), (20) and (21), respectively, after a finite number of terms. Specifically, we shall denote by $L_{\rm N}$ the number of terms that we retain in the series (19) and (20), and by $L_{\rm F}$ the number of terms that we retain in the series (21). In practice we take into account all the propagating modes and sufficiently many of the evanescent.

Goldstein in [2] proved optimal order error estimates in H^1 and L^2 norms for a similar discretization in the case of a homogeneous single-layer waveguide in Cartesian coordinates, and he studied the effect brought upon the error by the truncation of the series in the DtN operator. Analogous results for the case of an axisymmetric waveguide have been obtained in [18].

3.1 Implementation issues

We implemented the dicretization (23) in a Fortran code, referred to as FENL^2 in the sequel. This code is a modified version of the code called FENL, which was originally developed by Kampanis and Dougalis and implemented a finite element method coupled with a DtN condition posed on the artificial outflow boundary Γ_2. FENL is described in detail in [15]. Here we shall briefly describe FENL^2, especially some of the various changes or additions that were performed in FENL.

3.1.1 Triangulation of the domain

To triangulate the domain Ω we use the APNOPO module of the MODULEF library, [19]. This general module selects various other modules to create and modify the mesh. Specifically, we use the modules TRIGEO, which generates a triangular mesh with the use of an advancing front method, or TRIHER, which corresponds to a Voronoi method. From the modification modules we have mainly used RETRIN to refine the mesh, REGMA2 to regularize the mesh, and GIBBS to renumber the nodes of the mesh. For more information on these modules we refer to [20]. The output of APNOPO is a NOPO data structure, which in turn is read by an appropriate subroutine of FENL^2, which provides the information required for the assembly of the finite element matrices.

3.1.2 Assembly of the finite element matrices

We shall begin the assembly of the finite element matrices without imposing the Dirichlet boundary conditions in our variational formulation. Hence we consider the finite element space

$V_h := \{\phi :\ \phi \in C(\overline{\Omega}),\ \phi\,|_\tau \in \mathbb{P}_1\ \ \forall\, \tau \in \mathcal{T}_h\}$. Let $N_{\rm nd}$ be the number of nodes of the triangulation $\mathcal{T}_h$ and $\{\varphi_i\}_{i=1,\ldots,N_{\rm nd}}$ be the usual finite element basis. Now, letting $u_h = \sum_{j=1}^{N_{\rm nd}} u_j \varphi_j$ and $\phi = \varphi_i$, $i = 1, \ldots, N_{\rm nd}$, in (23), we end up with the linear system

$$(-\mathcal{G} + \mathcal{Q} + \mathcal{B} - \mathcal{C})\, \boldsymbol{u} = \boldsymbol{s}, \tag{24}$$

where $\mathcal{G}$, $\mathcal{Q}$, $\mathcal{B}$ and $\mathcal{C}$ denote the $N_{\rm nd} \times N_{\rm nd}$ matrices with entries

$$\mathcal{G}_{ij} = (\nabla\varphi_j, \nabla\varphi_i)_{L^2_\rho(\Omega)}, \quad \mathcal{Q}_{ij} = (k^2\varphi_j, \varphi_i)_{L^2_\rho(\Omega)},$$
$$\mathcal{B}_{ij} = (\widetilde{T}(\varphi_j), \varphi_i)_{L^2_\rho(\Gamma_2)}, \quad \mathcal{C}_{ij} = (\widetilde{R}(\varphi_j), \varphi_i)_{L^2_\rho(\Gamma_4)},$$

and $\boldsymbol{s}$ the (column) vector with components $s_i = (\widetilde{S}, \varphi_i)_{L^2_\rho(\Gamma_4)}$.

We should like to note that at this level the system (24) is not equivalent to (23) since it remains to impose the Dirichlet boundary conditions on u_h.

The entries of the stiffness matrix $\mathcal{G}$ and the mass matrix $\mathcal{Q}$ are computed as is done in the prototype FENL, refer to [15] for details. Now, in order to compute the entries of the matrices $\mathcal{B}$ and $\mathcal{C}$ and the vector $\boldsymbol{s}$, we have to compute the eigenvalues and the eigenvectors of the vertical eigenvalue problem (11)-(15), where $*$ is F or N depending on whether we work on Γ_2 or Γ_4. In FENL the vertical eigenvalue problem was solved with the standard Galerkin/finite element method with continuous, piecewise linear functions on the partition induced on Γ_2 by the triangulation $\mathcal{T}_h$. To solve it, routines from EISPACK, [21], were used. During this procedure some extra care had to be taken to choose the discretization parameter δz on Γ_2 sufficiently small in order to obtain good approximations of the actual eigenpairs, since the number of the numerically acceptable eigenpairs, which is less or equal to the dimension of the finite element space on Γ_2, is inversely depending on the discretization parameter δz, cf. [22]. This kind of approach may possibly lead to very fine grids near the artificial boundaries when the number of modes that contribute in $\widetilde{R}$, $\widetilde{S}$ and $\widetilde{T}$ is large. To avoid this, in FENL^2, we have calculated the eigenpairs $\{\lambda^{\rm N}_{h,n}, Z^{\rm N}_{h,n}\}$ and $\{\lambda^{\rm F}_{h,n}, Z^{\rm F}_{h,n}\}$ of the vertical eigenvalue problems on Γ_4 and Γ_2, respectively, in a sufficiently fine grid ensuring that we obtained good approximations of all the propagating and the most significant of the evanescent modes, and then we evaluate them on the boundary nodes induced by the triangulation $\mathcal{T}_h$ by linear interpolation. Now, let $\{1, 2, \ldots, M_{\rm N}\}$ be a successive numbering of all the nodes lying on the inflow boundary Γ_4 excluding the node $(R_1, 0)$, and $\{1, 2, \ldots, M_{\rm F}\}$ be a successive numbering of all the nodes lying on the outflow boundary Γ_2 excluding the node $(R_2, 0)$. Let also j_ℓ denotes the global number

in $\mathcal{T}_h$ of the ℓth node ($1 \le \ell \le M_{\rm N}$) that lies on Γ_4 and m_ℓ denotes the global number in $\mathcal{T}_h$ of the ℓth node ($1 \le \ell \le M_{\rm F}$) that lies on Γ_2. Then the eigenvector $Z^{\rm N}_{h,n}$ corresponding to the inflow approximate eigenvalue $\lambda^{\rm N}_{h,n}$ may be written as $Z^{\rm N}_{h,n} = \sum_{\ell=1}^{M_{\rm N}} c_{n,\ell}\varphi_{j_\ell}|_{\Gamma_4}$, and, similarly, the eigenvector $Z^{\rm F}_{h,n}$ corresponding to the outflow approximate eigenvalue $\lambda^{\rm F}_{h,n}$ may be written as $Z^{\rm F}_{h,n} = \sum_{\ell=1}^{M_{\rm F}} d_{n,\ell}\varphi_{m_\ell}|_{\Gamma_2}$. Now we are in a position to write the (i,m) entry of matrix $\mathcal{B}$, the (i,j) entry of matrix $\mathcal{C}$ and the ith component of the vector $\boldsymbol{s}$ in the following form

$$
\begin{aligned}
\mathcal{B}_{im} &= \Big(\widetilde{T}(\varphi_m),\varphi_i\Big)_{L^2_\rho(\Gamma_2)} = \\
&= \sum_{n=1}^{L_{\rm F}} B_{h,n}\left(\sum_{\ell=1}^{M_{\rm F}} d_{n,\ell}\left(\varphi_m(R_2,\cdot),\varphi_{m_\ell}(R_2,\cdot)\right)_{L^2_\rho(0,H_{\rm F})}\right)\left(\sum_{\ell=1}^{M_{\rm F}} d_{n,\ell}\left(\varphi_{m_\ell},\varphi_i\right)_{L^2_\rho(\Gamma_2)}\right), \quad (25)\\
\mathcal{C}_{ij} &= \Big(\widetilde{R}(\varphi_j),\varphi_i\Big)_{L^2_\rho(\Gamma_4)} = \\
&= \sum_{n=1}^{L_{\rm N}} C_{h,n}\left(\sum_{\ell=1}^{M_{\rm N}} c_{n,\ell}\left(\varphi_j(R_1,\cdot),\varphi_{j_\ell}(R_1,\cdot)\right)_{L^2_\rho(0,H_{\rm N})}\right)\left(\sum_{\ell=1}^{M_{\rm N}} c_{n,\ell}\Big(\varphi_{j_\ell},\varphi_i\Big)_{L^2_\rho(\Gamma_4)}\right), \quad (26)\\
s_i &= \Big(S,\varphi_i\Big)_{L^2_\rho(\Gamma_4)} = -\frac{1}{2\pi\rho_1 R_1}\sum_{n=1}^{L_{\rm N}} S_{h,n}\, Z^{\rm N}_{h,n}(z_s)\left(\sum_{\ell=1}^{M_{\rm N}} c_{n,\ell}\Big(\varphi_{j_\ell},\varphi_i\Big)_{L^2_\rho(\Gamma_4)}\right), \quad (27)
\end{aligned}
$$

where

$$
B_{h,n} := \begin{cases} -\sqrt{\lambda^{\rm F}_{h,n}}\,\dfrac{H^{(1)}_1\Big(\sqrt{\lambda^{\rm F}_{h,n}}\,R_2\Big)}{H^{(1)}_0\Big(\sqrt{\lambda^{\rm F}_{h,n}}\,R_2\Big)}, & \text{if } \lambda^{\rm F}_{h,n} > 0 \\ -\sqrt{-\lambda^{\rm F}_{h,n}}\,\dfrac{K_1\Big(\sqrt{-\lambda^{\rm F}_{h,n}}\,R_2\Big)}{K_0\Big(\sqrt{-\lambda^{\rm F}_{h,n}}\,R_2\Big)}, & \text{if } \lambda^{\rm F}_{h,n} < 0 \end{cases},
$$

$$
C_{h,n} := \begin{cases} -\sqrt{\lambda^{\rm N}_{h,n}}\,\dfrac{J_1\Big(\sqrt{\lambda^{\rm N}_{h,n}}\,R_1\Big)}{J_0\Big(\sqrt{\lambda^{\rm N}_{h,n}}\,R_1\Big)}, & \text{if } \lambda^{\rm N}_{h,n} > 0 \\ \sqrt{-\lambda^{\rm N}_{h,n}}\,\dfrac{I_1\Big(\sqrt{-\lambda^{\rm N}_{h,n}}\,R_1\Big)}{I_0\Big(\sqrt{-\lambda^{\rm N}_{h,n}}\,R_1\Big)}, & \text{if } \lambda^{\rm N}_{h,n} < 0, \end{cases},
$$

and

$$
S_{h,n} := \begin{cases} \dfrac{1}{J_0\Big(\sqrt{\lambda^{\rm N}_{h,n}}\,R_1\Big)}, & \text{if } \lambda^{\rm N}_{h,n} > 0 \\ \dfrac{1}{I_0\Big(\sqrt{-\lambda^{\rm N}_{h,n}}\,R_1\Big)}, & \text{if } \lambda^{\rm N}_{h,n} < 0 \end{cases}.
$$

Here I_ν and K_ν are the modified Bessel functions of the first and second kind, respectively. The values of the special functions involved in the above formulas are computed with the aid of Fortran subroutines in double precision from the SPECFUN 2.5 library which is freely available from NETLIB (`http://www.netlib.org/`).

Finally, to impose the Dirichlet boundary conditions we follow the same technique as in FENL. If a_j denotes a node belonging to Γ_3, then the jth component of the vector $\boldsymbol{u}$ is zero. This is implemented by setting the jth row and column of the matrix $-\mathcal{G}+\mathcal{Q}+\mathcal{B}-\mathcal{C}$ equal to zero, its (j,j) entry equal to 1, and the jth component of the vector $\boldsymbol{s}$ equal to zero.

3.1.3 Solving the linear system

The resulting linear system is large, sparse, indefinite and complex symmetric, and is solved with methods from the QMRPACK software package, [23]. QMRPACK contains implementations of various Quasi-Minimal Residual (QMR) iterative algorithms, cf. [24]. These are iterative schemes that belong to the general class of Krylov subspace methods, involve few–term recurrences, and are applicable to systems with nonsingular, complex, not necessarily Hermitian matrices. In our tests in the present paper we have mainly used the double precision complex version of CPL, which is based on the coupled two-term Lanczos with look-ahead, cf. [25]. From the built-in preconditioners of QMRPACK we have experimented mainly with two-sided SSOR and two-sided ILUT. We would like to report that we have noticed that the numbering of the nodes of the triangulations and, hence, the sparsity pattern of the coefficient matrix played an important role to the linear system solver, especially when preconditioners based on incomplete factorization were used. We refer to Benzi et al., [26], for details concerning this phenomenon. Thus, in all cases extra care was taken, and a reordering module of MODULEF was used, in order to decrease the bandwidth of the coefficient matrix and, consequently, improve the efficiency of the preconditioner. We should also like to note here that most of the computational effort of the finite element method is devoted in solving the linear system.

Finally, to produce one- or two-dimensional plots we used MATLAB's PDE Toolbox, [27], with the aid of a routine which exports the data (triangulation information and solution at the nodes) from FENL^2 in the appropriate format needed by the graphics module.

4 Numerical experiments

In this section we present the outcome of some numerical experiments that we performed with the code FENL^2 in stratified marine environments with variable interface. In all cases we compare our results with COUPLE. (For a detailed comparison of the prototype FENL with other coupled mode methods refer to [17].) Here we shall examine three cases corresponding

to interfaces that simulate an upslope, a downslope and an underwater hill environment. In all cases the densities and the sound speeds of the seawater and the sediment are taken constant and equal to $\rho_{\rm w} = 1.0$ g/cm^3, $c_{\rm w} = 1500$ m/sec in the water layer and $\rho_{\rm s} = 1.5$ g/cm^3, $c_{\rm s} = 1700$ m/sec in the sediment. The hard horizontal bottom is placed at a depth equal to 100 m. We have experimented with relatively low source frequencies up to 50 Hz, in order to keep the computational demands in fairly low levels, since it is well known that the error in the finite element solution grows as the frequency increases and the discretization parameter h and the wavenumber k should be adjusted in order to achieve a given accuracy level. In fact, many authors follow a rule of the form $kh = $ const., by assuming a constant number of elements (usually ten) per wavelength. However, it has been found that this is not enough as the frequency (and, consequently, the wavenumber) increases, and that the error in the L^2 norm remains bounded when k^3h^2 is kept constant, while it grows with k for $kh = $ const.. This result has been numerically verified by Bayliss et al., [28], [29], for two-dimensional model problems in Cartesian coordinates, and more recently by Oberai and Pinsky, [30], for more general problems and non-uniform meshes. Ihlenburg and Babuška, [31], provide analytical estimates for a one-dimensional model problem which indicate that it suffices to keep k^3h^2 constant in order to avoid a growth of the relative L^2-error. For more details we refer to the book of Ihlenburg, [32].

In all examples we ran COUPLE with a range step $\delta r = 1.0$ m, and the number of the contributing modes was taken equal to 15. (The rigid bottom in COUPLE was simulated by assuming very large values for the density and the sound speed in the semi-infinite layer used by COUPLE.) In all FENL^2 runs the far-field boundary was posed at $R_2 = 750$ m, and as a linear system solver we used CPL of QMRPACK, combined with the two-sided SSOR preconditioner with parameter $\omega = 1.2$. In all examples we shall report the size of the grid used by FENL^2, the value of R_1, i.e. the distance where the near-field boundary condition is posed, the number of modes that propagate at the artificial boundaries, the number of modes that were taken into account in the calculation of the near-field and the far-field boundary condition, denoted by $L_{\rm N}$ and $L_{\rm F}$, respectively (see the formulas (25)–(27)). We shall also report the number of iterations and the CPU-time that the linear system solver needed to converge, and the values of $\xi_{\rm w}$ and $\xi_{\rm s}$, where ξ_i is an indicative parameter measuring the number of average size meshlengths contained in a wavelength in the water ($i = $ w) or the sediment ($i = $ s), for constant sound speeds $c_{\rm w} = 1500$ m/sec and $c_{\rm s} = 1700$ m/sec in the two media. We would like to note that care has been taken and R_1 has been chosen so that $\sqrt{\lambda^{\rm N}_{h,n}}R_1$ is not a root of the Bessel function J_0, for

$n = 1, 2, \ldots, N_{\rm N}$, where $N_{\rm N}$ is the number of modes that propagate at $r = R_1$. All the FENL^2 runs were performed on a Pentium IV PC with a RAM of 1 GB running under Linux at 2.4 GHz.

Example 1: Upslope. As a first example we consider the case of an upslope interface defined by the curve

$$h(r) = \begin{cases} 75 & , \quad \text{for } 0 < r \leq 300, \\ 50 - 25 \sin \frac{2\pi(r-500)}{800} & , \quad \text{for } 300 < r < 700, \\ 25 & , \quad \text{for } r \geq 700. \end{cases}$$

(All distances are in meters.) The source is placed at a depth equal to 20 m and the near-field boundary is posed at $R_1 = 250$ m. In Figure 2 we present two-dimensional transmission loss plots obtained by the COUPLE and the FENL^2 codes, for a frequency $f = 25$ Hz.

Figure 2 is here.

Figure 3 shows superimposed one-dimensional plots of transmission loss vs. range at a receiver depth $RD = 50$ m. (This plot was extracted from the run that gave the 2D plots of Figure 2.) The results are in excellent agreement. For the FENL^2 run we used a triangular mesh consisting of 40896 elements and 20809 nodes ($\xi_{\rm w} = 38$, $\xi_{\rm s} = 43$). Three modes propagate both at the near-field and at the far-field boundary. We took $L_{\rm N} = 10$ and $L_{\rm F} = 5$. The linear system solver required 712 iterations and 19 secs of CPU time to converge.

Figure 3 is here.

In order to give some idea for the convergence of the iterative solver we plot in Figure 4 the convergence curve, i.e. the relative residual norm vs. the number of iterations. As a convergence criterion we took the relative residual norm to be less than 10^{-12}. The behaviour presented in Figure 4 is quite typical in all the test cases examined in this paper, therefore we shall not include such figures for the rest of the examples.

Figure 4 is here.

Figures 5 and 6 show two- and one-dimensional transmission loss plots obtained by COUPLE and FENL^2 for a higher frequency of $f = 50$ Hz. Now, six modes propagate at the artificial boundaries and $L_{\rm N} = 15$ and $L_{\rm F} = 7$. The triangular mesh was consisting of 72704 elements and 36833 nodes ($\xi_{\rm w} = 26$, $\xi_{\rm s} = 29$). The linear system solver required 2621 iterations and 120 secs of CPU time to converge. The results again compare very well.

Figure 5 is here.

Figure 6 is here.

Example 2: Downslope. In a second example we consider the case of a downslope interface defined by the curve

$$h(r) = \begin{cases} 25 & , \quad \text{for } 0 < r \leq 300, \\ 50 + 25 \sin \frac{2\pi(r-500)}{800} & , \quad \text{for } 300 < r < 700, \\ 75 & , \quad \text{for } r \geq 700, \end{cases}$$

(All distances are in meters.) The source is placed at a depth equal to 20 m and $R_1 = 250$ m. Figure 7 shows two-dimensional transmission loss plots obtained by the COUPLE and the FENL^2 codes, for a frequency $f = 25$ Hz.

Figure 7 is here.

In Figure 8, the superimposed one-dimensional plots of transmission loss vs. range at a receiver depth $RD = 50$ m confirm the excellent agreement between the results of the two codes. For the FENL^2 run we used a triangular mesh consisting of 40896 elements and 20809 nodes ($\xi_{\rm w} = 38$, $\xi_{\rm s} = 43$). At the artificial boundaries three modes propagate. We took $L_{\rm N} = 10$ and $L_{\rm F} = 5$. The linear system solver required 730 iterations and 19 secs of CPU time to converge.

Figure 8 is here.

Figures 9 and 10 show two- and one-dimensional transmission loss plots obtained by COUPLE and FENL^2 for an increased frequency of $f = 50$ Hz. Here $L_{\rm N} = 15$ and $L_{\rm F} = 7$. The triangular mesh was consisting of 72704 elements and 36833 nodes ($\xi_{\rm w} = 26$, $\xi_{\rm s} = 29$). The linear system solver required 2025 iterations and 93 secs of CPU time to converge. The results again compare very well.

Figure 9 is here.

Figure 10 is here.

Example 3: Hill. In this last example we would like to assess the significance of incorporating this new near-field condition. To this end we shall compare the results obtained by FENL^2, with those of COUPLE, and also with those obtained by the prototype FENL. Now the interface forms an underwater hill given by

$$h(r) = \begin{cases} 50 - 25\cos\frac{2\pi(r-500)}{400} & , \quad \text{for } 300 < r < 700, \\ 75 & , \quad \text{elsewhere.} \end{cases}$$

(All distances are in meters.) The source is placed at a depth equal to 25 m, and the frequency is equal to $f = 27.80$ Hz. In order to run FENL we have used as a near-field condition (on $r = R_1$) a Dirichlet boundary condition of the form $u(R_1, z) = g(z)$, where $g(z)$ is the field obtained by COUPLE at $r = R_1$.

Figure 11 shows superimposed one-dimensional TL plots for a receiver depth $RD = 50$ m obtained by the three codes when $R_1 = 100$ m. For FENL and FENL^2 runs we have used exactly the same grid consisting of 52632 elements and 26767 nodes ($\xi_{\rm w} = 34$, $\xi_{\rm s} = 39$). The linear system solver, for the FENL run, required 1456 iterations and 48 secs of CPU time to converge, while for the FENL^2 run the corresponding values were 1324 iterations and 44 secs. The reader may immediately verify that the results of FENL^2 are in excellent agreement with those of COUPLE, while there is some discrepancy with those obtained by FENL.

Figure 11 is here.

Next we run the three codes with the near-field boundary posed at $R_1 = 150$ m. Now the grid used by FENL and FENL^2 consists of 48492 elements and 24667 nodes ($\xi_{\rm w} = 34$, $\xi_{\rm s} = 39$). For the FENL run the linear system solver required 1069 iterations and 33 secs of CPU time to converge, and 1001 iterations and 31 secs for the FENL^2 run. Figure 12 shows superimposed TL plots for a receiver depth $RD = 50$ m. Now the results of the three codes compare very well.

Figure 12 is here.

This kind of dependence of FENL's results on R_1, for some source frequencies, when data from coupled mode codes are used as a starting field for FENL has been first discovered and studied in some detail in [17]. To be more specific, in [17], it has been noticed that in some cases, where the frequency was such that an eigenvalue of the vertical problem changed sign several times and remained small in a neighbourhood of the interface inhomogeneity, the accuracy of

FENL's results was depending on the position R_1 of the starting field. For the frequency of 27.80 Hz four modes propagate at the artificial boundaries but in the vicinity of the hill the fourth mode changes its character from propagating to evanescent and vice versa several times, since the fourth eigenvalue of the vertical problem changes sign there, see Figure 13. We refer to [17] for a detailed discussion of this phenomenon.

We would like to note that in the previous two examples the results obtained by FENL were in perfect agreement with those obtained by COUPLE and FENL^2.

Figure 13 is here.

5 Concluding remarks

We have presented a code named FENL^2 which implements a finite element method for the Helmholtz equation in an inhomogeneous cylindrically symmetric waveguide consisting of two fluid layers. The waveguide is bounded in depth by a rigid bottom. Part of the bottom and the interface is assumed to be range-dependent. The code discretizes efficiently near- and far-field boundary conditions posed on two artificial boundaries. The near-field condition is a nonhomogeneous DtN-type condition relating the field near the source to the field in the rest of the waveguide. The far-field condition is obtained by the classical DtN map of the associated exterior problem. The code FENL^2 is a modified version of a prototype code called FENL. The main new ingredient in FENL^2 is the introduction and implementation of a near-field boundary condition. This new feature is of some importance since it makes FENL^2 a self-contained finite element code, in the sense that it does not depend on data given by other codes on the near-field boundary, as opposed to the prototype FENL. The code has been successfully tested and compared to COUPLE in various small scale examples and for relatively low values of source frequency. The main restriction in the current version of the code comes from the triangulator, i.e. our Fortran implementation of MODULEF, which may handle a moderate number of elements and nodes. In the future we intend to experiment with other triangulators that produce, and are capable of handling, larger meshes.

Future work includes the replacement of the rigid bottom assumption by a more realistic one and the addition of attenuation (absorption) in the medium. Ideally, the lowest boundary should not reflect any acoustic energy back, hence a complete formulation would, perhaps, entail posing at the bottom another suitable absorbing condition.

Acknowledgement: The author would like to thank two unnamed referees of the first version of this paper for their comments and suggestions and to gratefully acknowledge partial support for this research from a "Pythagoras" EPEAEK II grant to the University of Athens, which was co-funded by the EU European Social Fund and national resources.

Figures

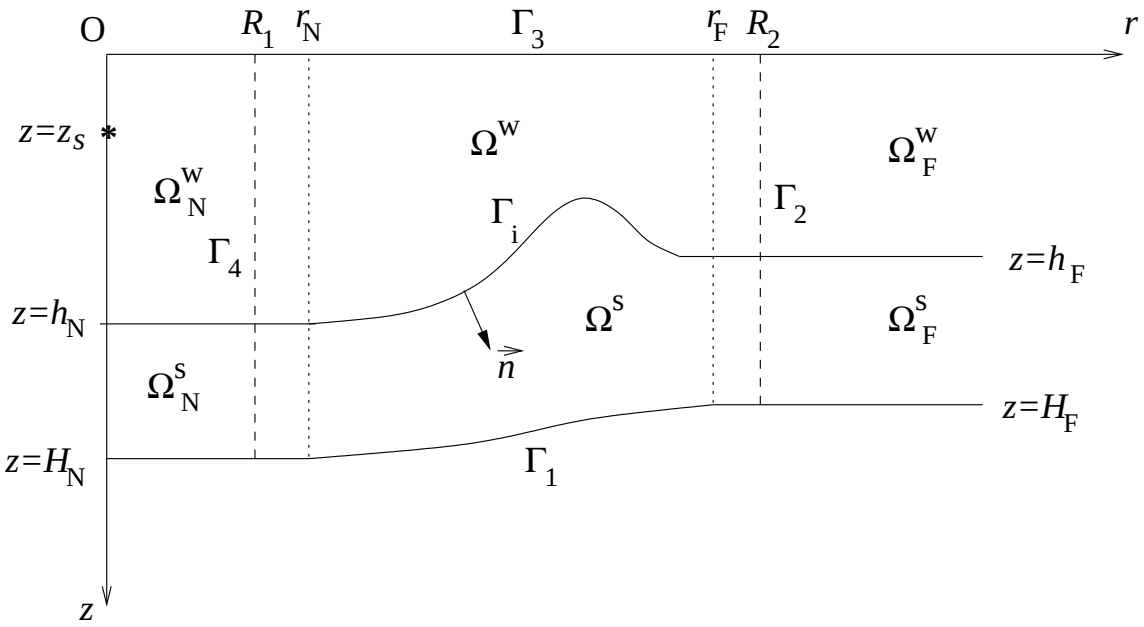

Figure 1: Domain of interest and basic notation.

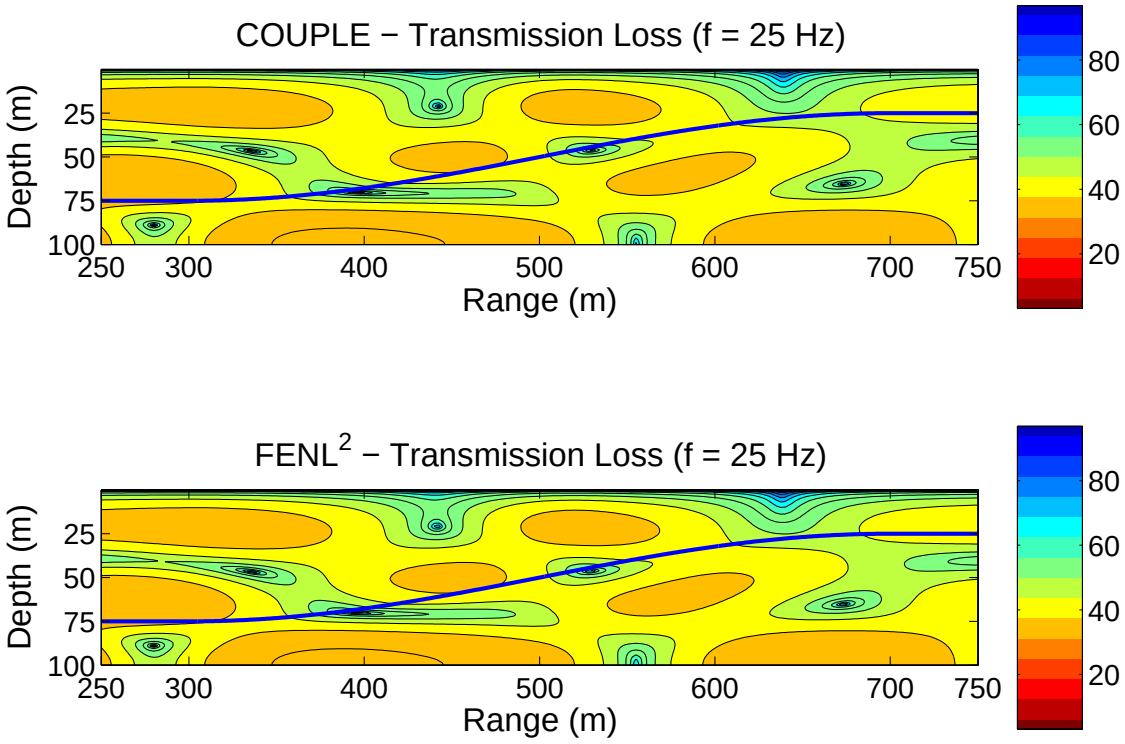

Figure 2: Upslope. Transmission loss plots of COUPLE and FENL^2. $f = 25$ Hz.

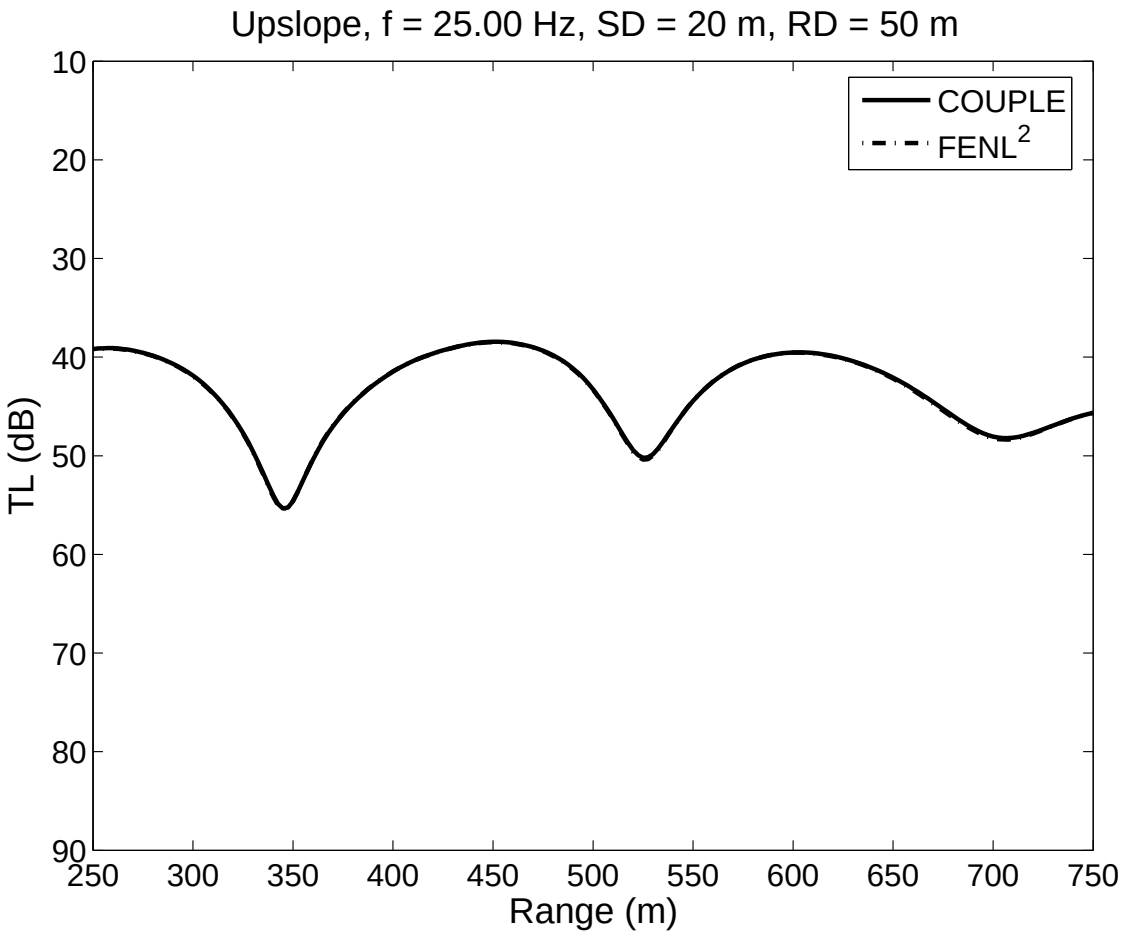

Figure 3: Upslope. $f = 25$ Hz. Comparison between COUPLE and FENL^2 at a receiver depth of 50 m.

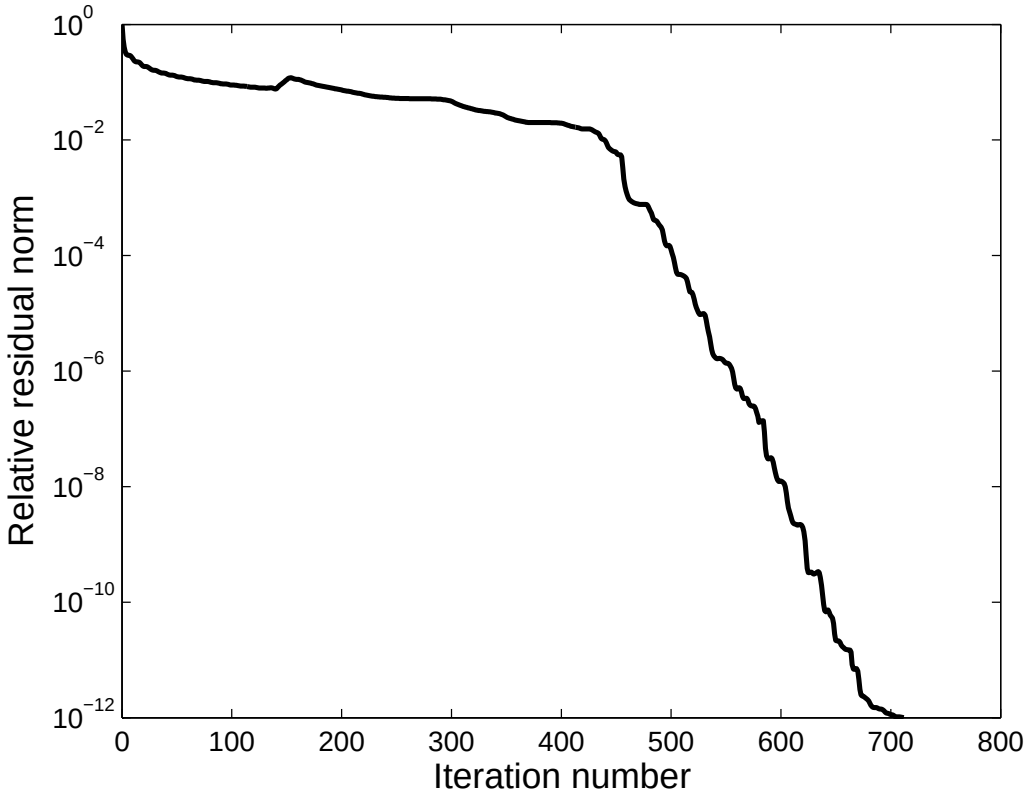

Figure 4: Upslope, $f = 25$ Hz.

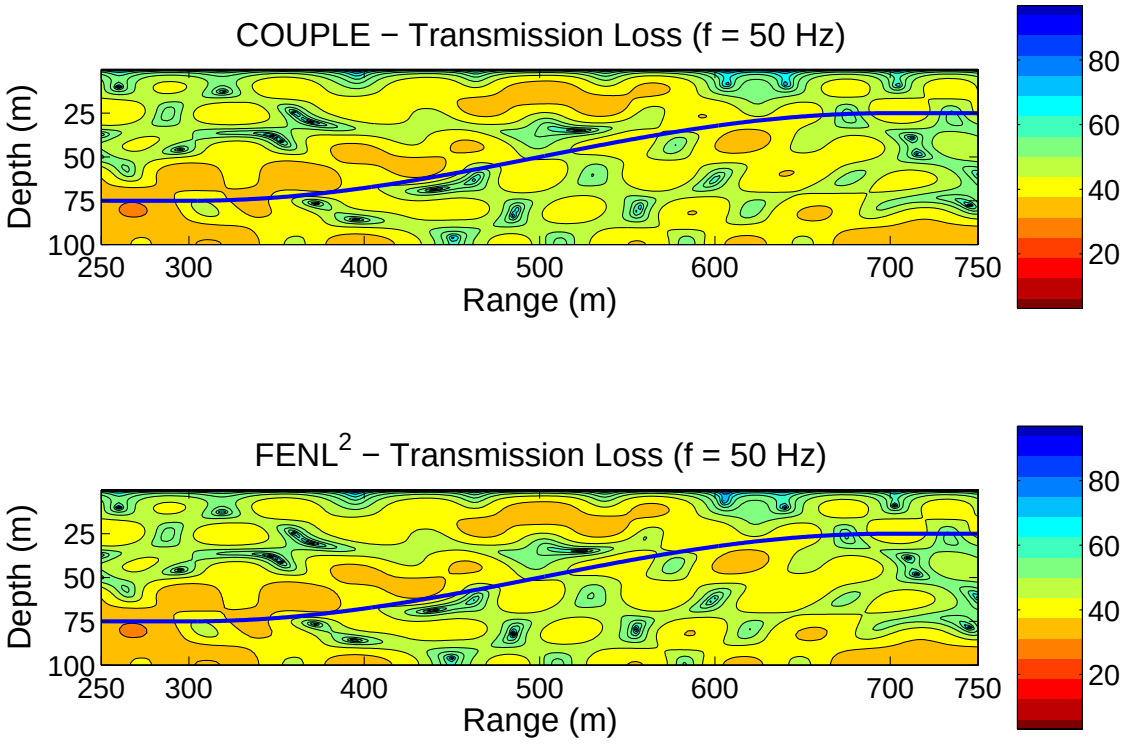

Figure 5: Upslope. Transmission loss plots of COUPLE and FENL^2. $f = 50$ Hz.

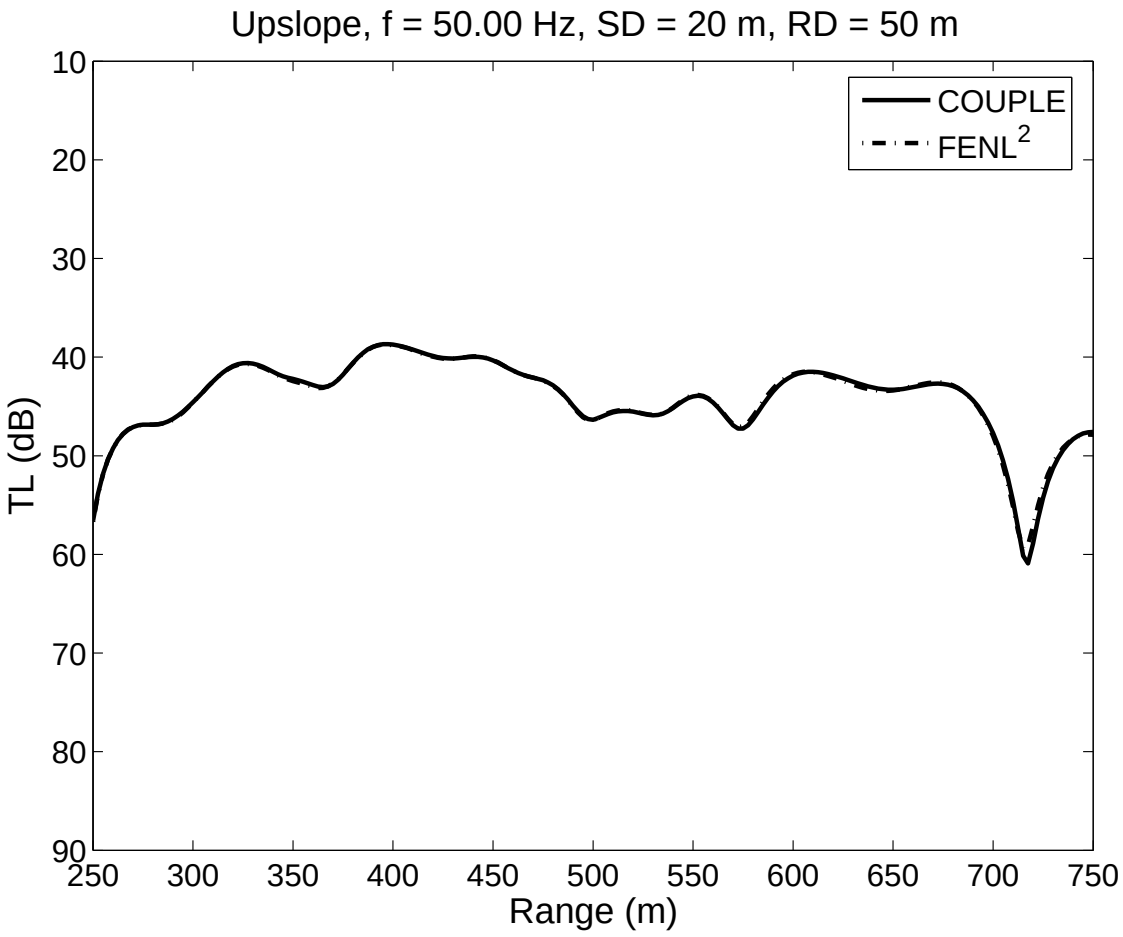

Figure 6: Upslope. $f = 50$ Hz. Comparison between COUPLE and FENL^2 at a receiver depth of 50 m.

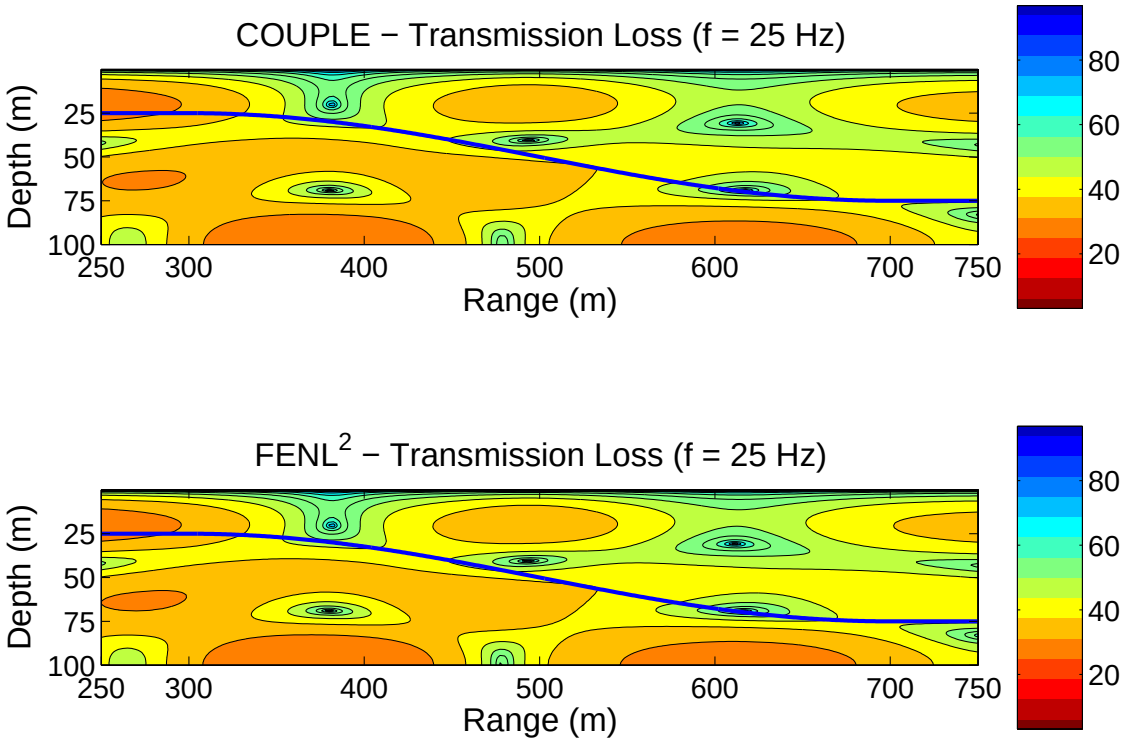

Figure 7: Downslope. Transmission loss plots of COUPLE and FENL^2. $f = 25$ Hz.

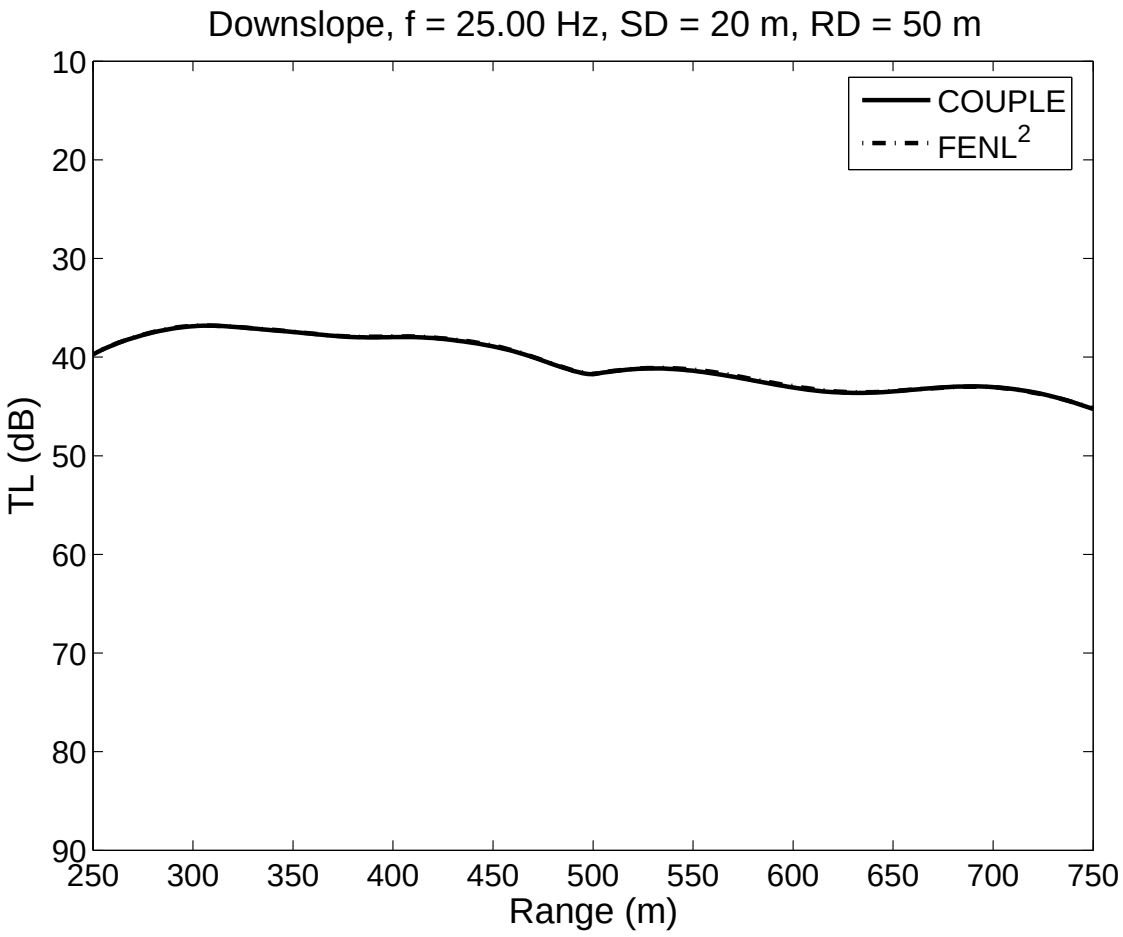

Figure 8: Downslope. $f = 25$ Hz. Comparison between COUPLE and FENL^2 at a receiver depth of 50 m.

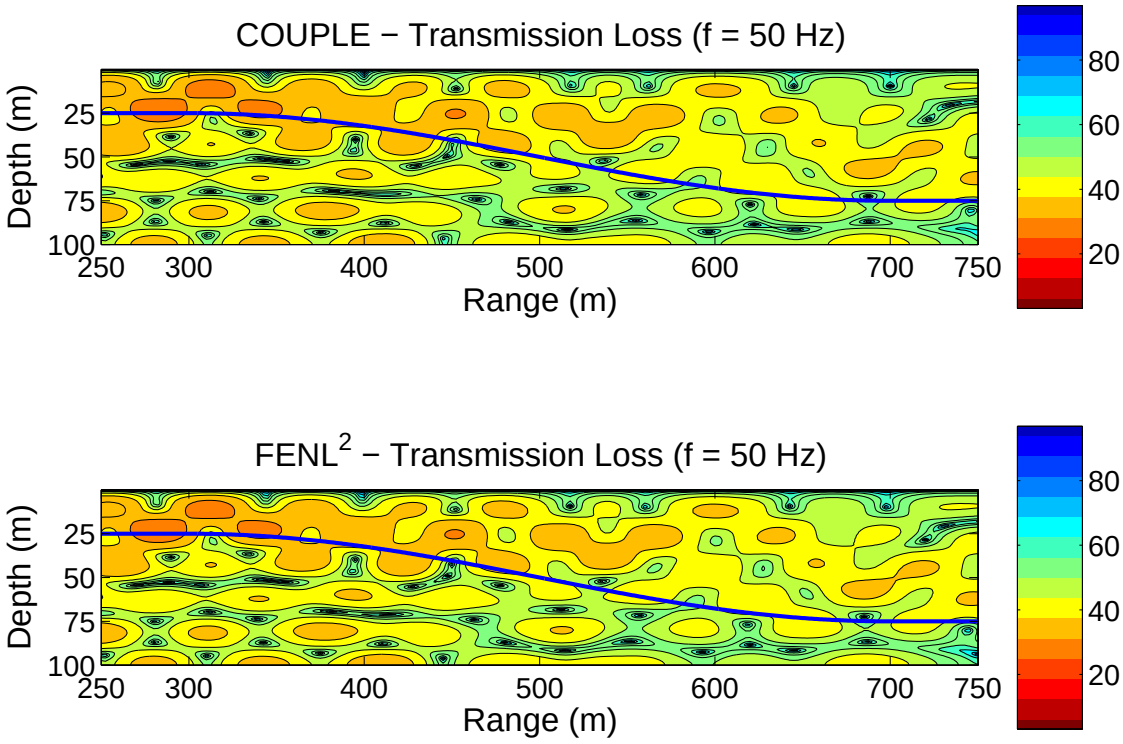

Figure 9: Downslope. Transmission loss plots of COUPLE and FENL^2. $f = 50$ Hz.

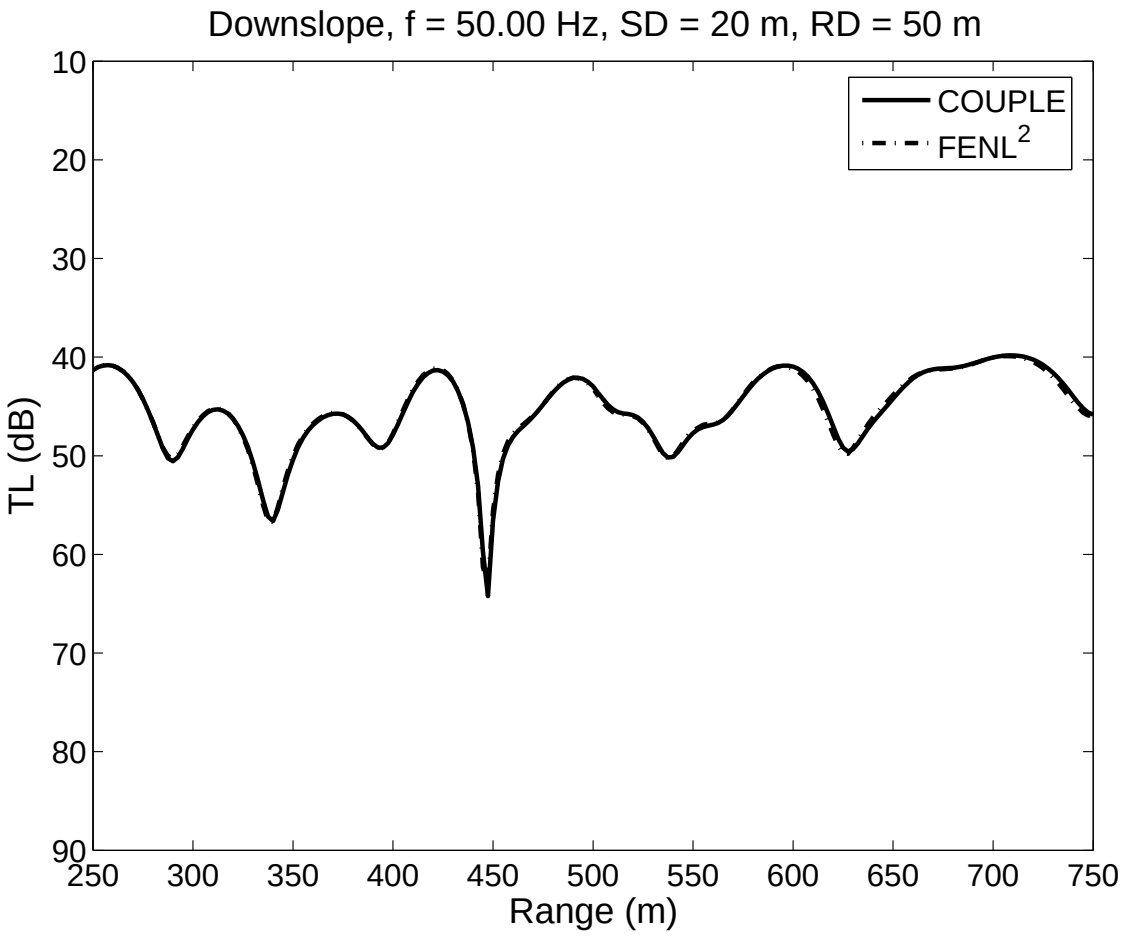

Figure 10: Downslope. $f = 50$ Hz. Comparison between COUPLE and FENL^2 at a receiver depth of 50 m.

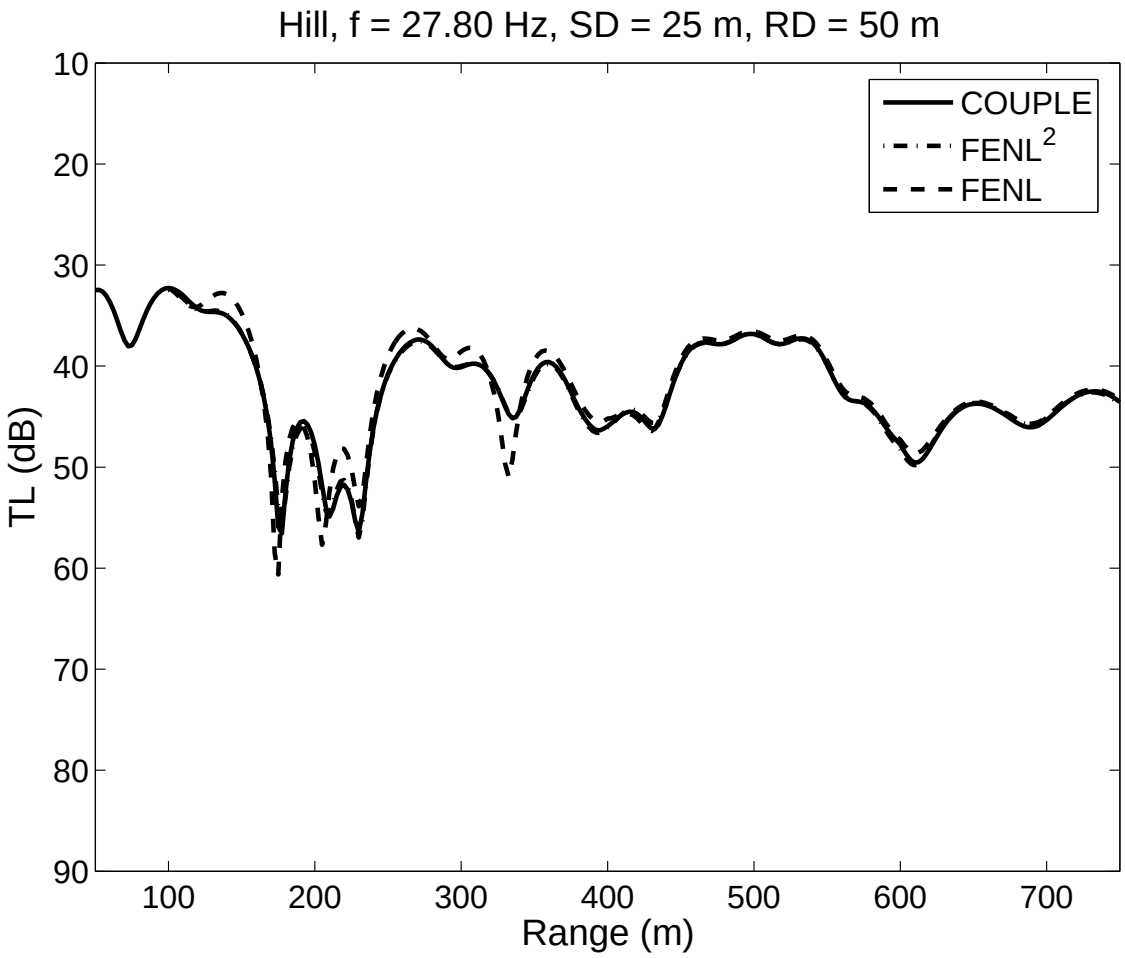

Figure 11: Hill. Transmission loss plots of COUPLE, FENL^2 and FENL. $f = 27.80$ Hz, $R_1 = 100$ m.

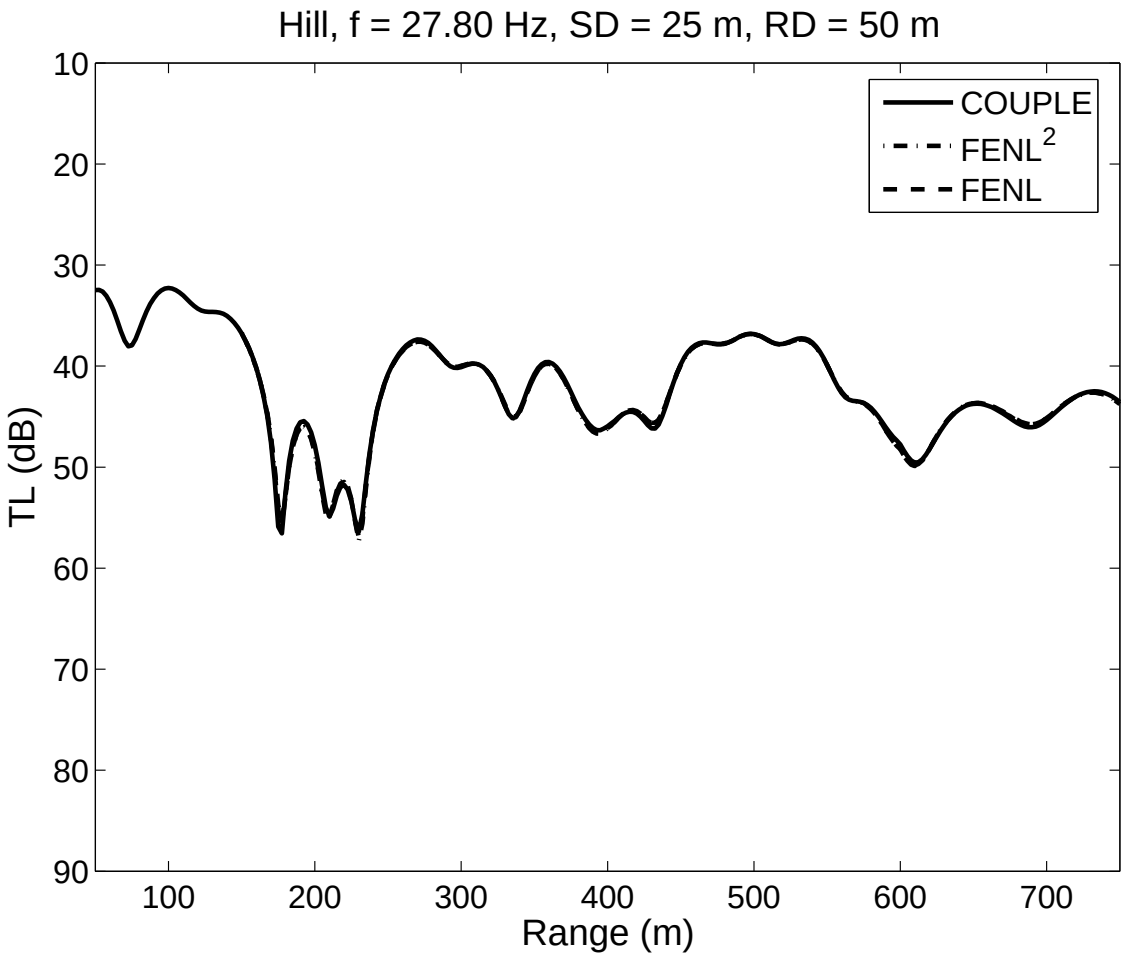

Figure 12: Hill. Transmission loss plots of COUPLE, FENL^2 and FENL. $f = 27.80$ Hz, $R_1 = 150$ m.

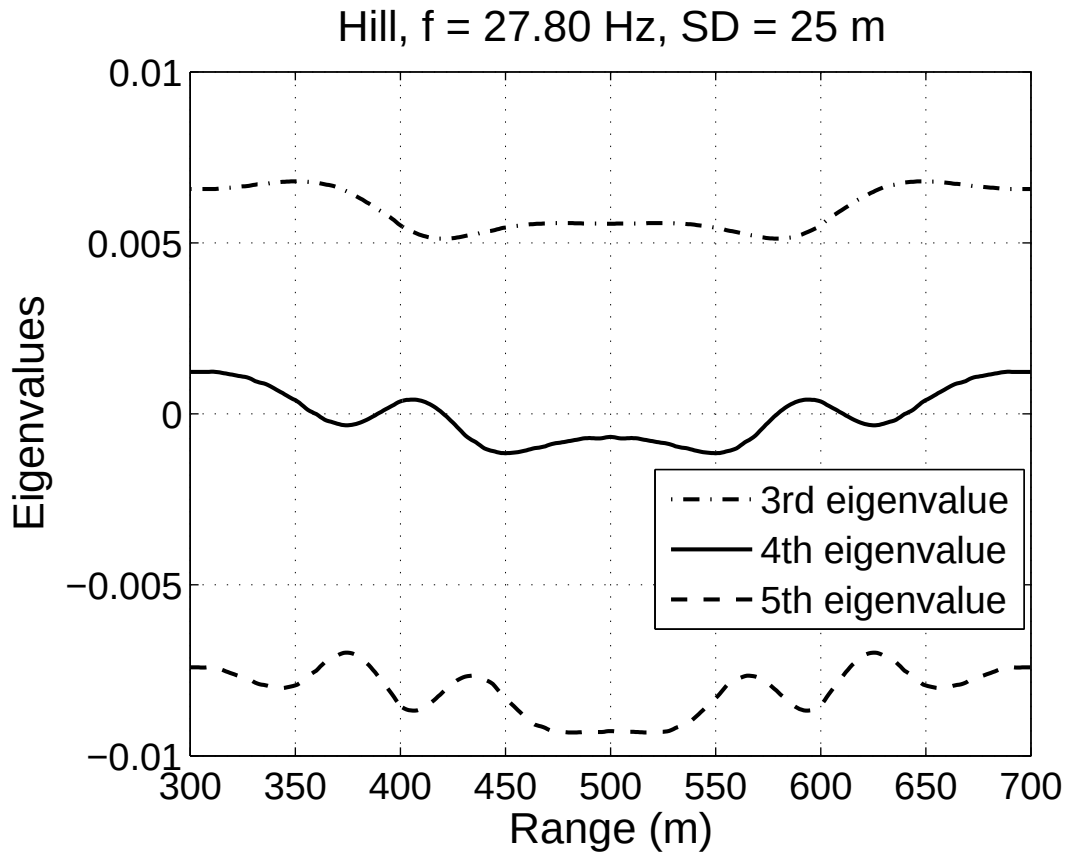

Figure 13: Hill. $f = 27.80$ Hz. Three eigenvalues of the vertical problem and their dependence on r.

References

[1] G. J. Fix, S. P. Marin, Variational methods for underwater acoustic problems, *J. Comp. Physics*, **28** (1978) 253–270.

[2] C. I. Goldstein, A finite element method for solving Helmholtz type equations in waveguides and other unbounded domains, *Math. Comp.*, **39** (1982) 309–324.

[3] J. B. Keller, D. Givoli, Exact non–reflecting boundary conditions, *J. Comp. Physics*, **82** (1989) 172–192.

[4] D. Givoli, *Numerical Methods for Problems in Infinite Domains*, Elsevier, 1992.

[5] L. L. Thompson, A review of finite-element methods for time-harmonic acoustics, *J. Acoust. Soc. Am.*, **119** (2005) 1315–1330.

[6] M. J. Buckingham, Ocean-acoustic propagation models, *J. Acoustique*, **3** (1992) 223–287.

[7] C. A. Boyles, *Acoustic Waveguides: Applications to Oceanic Science*, Wiley, 1984.

[8] F. B. Jensen, W. A. Kuperman, M. B. Porter, H. Schmidt, *Computational Ocean Acoustics*, American Institute of Physics, 1993.

[9] R. B. Evans, A coupled mode solution for the acoustic propagation in a waveguide with stepwise depth variations of a penetrable bottom, *J. Acoust. Soc. Am.*, **74** (1983) 188–195.

[10] R. B. Evans, COUPLE: a user's manual, NORDA TN–332, 1986.

[11] S. R. Rutherford, K. E. Hawker, Consistent coupled mode theory of sound propagation for a class of nonseparable problems, *J. Acoust. Soc. Am.*, **70** (1981) 554–564.

[12] M. I. Taroudakis, G. A. Athanassoulis, J. P. Ioannidis, A variational principle for underwater acoustic propagation in a three-dimensional ocean environment, *J. Acoust. Soc. Am.*, **88** (1990) 1515–1521.

[13] J. A. Fawcett, A derivation of the differential equations of coupled mode propagation, *J. Acoust. Soc. Am.*, **97** (1992) 290–295.

[14] G. A. Athanassoulis, K. A. Belibassakis, Rapidly-convergent local-mode representations for wave propagation and scattering in curved-boundary waveguides, in *Proc. 6th International Conference on Mathematical and Numerical Aspects of Wave Propagation (Waves 2003)*, G. C. Cohen. E. Heikkola, P. Joly, P. Neittaanmäki eds., Springer, 2003, 451–456.

[15] N. A. Kampanis, V. A. Dougalis, A finite element code for the numerical solution of the Helmholtz equation in axially symmetric waveguides with interfaces, *J. Comp. Acoustics*, **7** (1999) 83–110.

[16] V. A. Dougalis, N. A. Kampanis, M. I. Taroudakis, Comparison of finite element and coupled mode solutions of the Helmholtz equation in underwater acoustics, in *Proc. 4th European Conference in Underwater Acoustics*, eds. A. Alippi and G. B. Cannelli, CNR-IDAC, Rome 1998, Vol. II, pp. 649–654.

[17] G. A. Athanassoulis, K. A. Belibassakis, D. A. Mitsoudis, N. A. Kampanis, V. A. Dougalis, Coupled mode and finite element solutions of underwater sound propagation problems in stratified environments, *J. Comp. Acoustics*, to appear.

[18] D. A. Mitsoudis, Finite element methods for axisymmetric, indefinite boundary-value problems and applications in underwater acoustics (in Greek), Ph.D. Thesis, University of Athens, Greece, 2003.

[19] M. Bernadou, P. L. George, A. Hassim, P. Joly, P. Laug, A. Perronnet, E. Saltel, D. Steer, G. Vanderborck, M. Vidrascu: *MODULEF: A Modular Library of Finite Elements*, INRIA, 1988.

[20] P. L. George, *Automatic mesh generation: Application to finite element methods* Wiley, 1991.

[21] B. T. Smith, J. M. Boyle, B. S. Garbow, Y. Ikebe, V. C. Klema, C. B. Moler, *Matrix eigensystem routines – EISPACK guide*, Springer, 1976.

[22] I. Babuška, J. Osborn, Eigenvalue problems, in *Handbook of numerical analysis Vol. II*, eds. P. G. Ciarlet and J. L. Lions, Elsevier (1991) 641–787.

[23] R. W. Freund, N. M. Nachtigal, QMRPACK: A package of QMR Algorithms, *ACM Trans. Math. Software*, **22** (1996) 46–77.

[24] R. W. Freund, N. M. Nachtigal, QMR: a quasi–minimal residual method for non-Hermitian linear systems, *Numer. Math.*, **60** (1991) 315–339.

[25] R. W. Freund, N. M. Nachtigal, An implementation of the QMR method based on coupled two-term recurrences, *SIAM J. Sci. Comput.*, **15** (1994) 313–337.

[26] M. Benzi, D. B. Szyld, A. Van Duin, Orderings for incomplete factorization preconditioning for nonsymmetric problems, *SIAM J. Sci. Comput.*, **20** (1999) 1652–1670.

[27] *Partial differential equation toolbox user's guide (for use with MATLAB)*. The MathWorks Inc., 1996.

[28] A. Bayliss, C. I. Goldstein, E. Turkel, On accuracy conditions for the numerical computation of waves, *J. Comp. Physics*, **59** (1985) 396–404.

[29] A. Bayliss, C. I. Goldstein, E. Turkel, The numerical solution of the Helmholtz equation for wave propagation problems in underwater acoustics, *Comp. Maths. with Appls.*, **11** (1985) 655–665.

[30] A. A. Oberai, P. M. Pinsky, A numerical comparison of finite element methods for the Helmholtz equation, *J. Comput. Acoustics*, **8** (2000) 211–221.

[31] F. Ihlenburg, I. Babuška, Finite element solution of the Helmholtz equation with high wave number, Part I: The h-version of the FEM, *Computers Math. Applic.*, **30** (1995) 9–37.

[32] F. Ihlenburg, *Finite Element Analysis of Acoustic Scattering*, Springer, 1998.